

Si–H Bond Activation by Electrophilic Phosphinidene Complexes

Kandasamy Vaheesar, Timothy M. Bolton, Allan L. L. East, and Brian T. Sterenberg*

Department of Chemistry and Biochemistry, University of Regina, 3737 Wascana Parkway, Regina, Saskatchewan, Canada S4S 0A2

Received October 28, 2009

The terminal electrophilic phosphinidene complex [CpFe(CO)₂{PN-*i*-Pr₂}][AlCl₄] (**2**), generated via chloride abstraction from [CpFe(CO)₂{P(Cl)N-*i*-Pr₂}] (**1**), reacts with primary, secondary, and tertiary silanes to form the silyl phosphine complexes [CpFe(CO)₂{P(H)(SiR₃)N-*i*-Pr₂}][AlCl₄] (**3**, SiR₃ = SiPhH₂; **4**, SiR₃ = SiPh₂H; **5**, SiR₃ = SiEt₃), in which the phosphinidene has inserted into the Si–H bond. A computational study shows that the insertion is concerted and has a triangular transition state. The silyl phosphine complexes **3**, **4**, and **5** are very susceptible to nucleophilic attack, which leads to P–Si bond cleavage and formation of the bridging phosphido complex [{CpFe(CO)₂(μ-CO){μ-P(H)N-*i*-Pr₂}][AlCl₄] (**6**).

Introduction

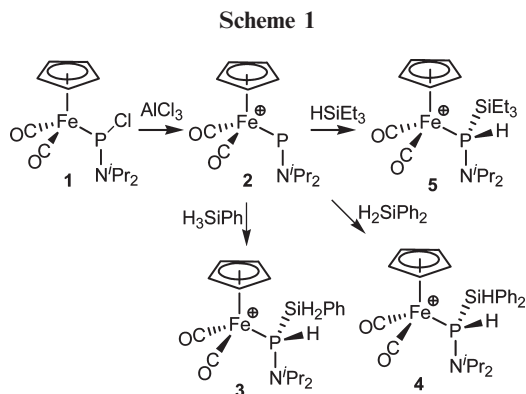
Transition metal terminal phosphinidene complexes can be considered analogous to transition metal carbene complexes, and like carbenes, their reactivity ranges between nucleophilic and electrophilic extremes.¹ Stable nucleophilic phosphinidenes have been known since 1987,² and characteristic reactivity of nucleophilic phosphinidenes includes [2+2] cycloaddition, nucleophilic attack by P, and protonation at P.³ The first electrophilic phosphinidenes were transient species generated *in situ*,⁴ and their reactivity has been well studied using trapping reactions with a wide variety of reagents.^{5,6} Characteristic reactions of electrophilic phosphinidenes include nucleophilic attack at P,^{7,8} [1+2] cycloadditions with unsaturated substrates,^{4,9} and bond insertions. In particular, insertion reactions of phosphinidenes into O–H and N–H bonds,⁴ strained C–N and C–O bonds,¹⁰ carbon–transition metal bonds,¹¹ and carbon–halogen bonds^{12,13} have been described. A few isolated

examples of C–H activation by terminal phosphinidene complexes have also been observed.¹⁴ Of these bond activation reactions, the one with the most potential synthetic utility is C–H activation. Carbene complexes, particularly transient carbene complexes generated by diazoalkane decomposition in the presence of metal catalysts, also undergo bond insertion reactions, and these reactions form the basis of a well-established synthetic methodology.¹⁵ More recently, stable electrophilic phosphinidenes have been isolated;^{9,16} however, their reactivity is not yet as well studied as that of the transient phosphinidenes.^{7,17–20} Here we discuss bond insertion reactions of the stable electrophilic terminal phosphinidene complex [CpFe(CO)₂{PN-*i*-Pr₂}][AlCl₄]. It belongs to a class of cationic phosphinidene complexes generated by chloride abstraction from chloro-phosphido ligands.^{9,16,18} These complexes are thermally stable and isolable, being stabilized by a heteroatom substituent that acts as a π-donor to the electron-deficient phosphorus atom. In contrast to the transient phosphinidenes W(CO)₅PR, which are generated by thermal decomposition of precursor complexes,^{5,6} stable, isolable phosphinidene complexes allow us to carry out reactions at room temperature or lower. Lower temperature reactions allow us to take a more detailed look at the mechanism of bond insertion reactions and can also be expected to lead to different reactivity. However, the

*Corresponding author. E-mail: brian.sterenberg@uregina.ca.

- (1) Cowley, A. H. *Acc. Chem. Res.* **1997**, *30*, 445.
- (2) Hitchcock, P. B.; Lappert, M. F.; Leung, W.-P. *J. Chem. Soc., Chem. Commun.* **1987**, 1282.
- (3) Stephan, D. W. *Angew. Chem., Int. Ed.* **2000**, *39*, 315.
- (4) Marinetti, A.; Mathey, F. *J. Am. Chem. Soc.* **1982**, *104*, 4484.
- (5) Lammertsma, K.; Vlaar, M. J. M. *Eur. J. Org. Chem.* **2002**, 1127.
- (6) Mathey, F.; Tran Huy, N. H.; Marinetti, A. *Helv. Chim. Acta* **2001**, *84*, 2938.
- (7) Sterenberg, B. T.; Udachin, K. A.; Carty, A. J. *Organometallics* **2001**, *20*, 4463.
- (8) Le Floch, P.; Marinetti, A.; Ricard, L.; Mathey, F. *J. Am. Chem. Soc.* **1990**, *112*, 2407.
- (9) Sánchez-Nieves, J.; Sterenberg, B. T.; Udachin, K. A.; Carty, A. J. *J. Am. Chem. Soc.* **2003**, *125*, 2404.
- (10) Marinetti, A.; Mathey, F. *Organometallics* **1987**, *6*, 2189.
- (11) Devaumas, R.; Marinetti, A.; Mathey, F.; Ricard, L. *J. Chem. Soc., Chem. Commun.* **1988**, 1325.
- (12) Khan, A. A.; Wismach, C.; Jones, P. G.; Streubel, R. *Chem. Commun.* **2003**, 2892.
- (13) Aysel, O.; Arif Ali, K.; Gerd, von F.; Martin, N.; Rainer, S. *Angew. Chem., Int. Ed.* **2007**, *46*, 2104. Tran Huy, N. H.; Mathey, F. *J. Org. Chem.* **2000**, *65*, 652.

- (14) Champion, D. H.; Cowley, A. H. *Polyhedron* **1985**, *4*, 1791. Svava, J.; Mathey, F. *Organometallics* **1986**, *5*, 1159. Tran Huy, N. H.; Compain, C.; Ricard, L.; Mathey, F. *J. Organomet. Chem.* **2002**, *650*, 57.
- (15) Wee, A. G. H. *Curr. Org. Synth.* **2006**, *3*, 499.
- (16) Sterenberg, B. T.; Udachin, K. A.; Carty, A. J. *Organometallics* **2001**, *20*, 2657. Sterenberg, B. T.; Udachin, K. A.; Carty, A. J. *Organometallics* **2003**, *22*, 3927.
- (17) Sterenberg, B. T.; Senturk, O. S.; Udachin, K. A.; Carty, A. J. *Organometallics* **2007**, *26*, 925.
- (18) Graham, T. W.; Cariou, R. P. Y.; Sanchez-Nieves, J.; Allen, A. E.; Udachin, K. A.; Regragui, R.; Carty, A. J. *Organometallics* **2005**, *24*, 2023.
- (19) Graham, T. W.; Udachin, K. A.; Carty, A. J. *Chem. Commun.* **2005**, 5890.
- (20) Graham, T. W.; Udachin, K. A.; Zgierski, M. Z.; Carty, A. J. *Can. J. Chem.* **2007**, *85*, 885.



stability of these complexes also has the disadvantage of lowering the reactivity, and the stabilized phosphinidenes are not generally electrophilic enough to activate C–H bonds directly. As a result, we looked for analogous but weaker X–H bonds to activate and have focused here on Si–H bond activation reactions. Transition metal phosphido and phosphinidene complexes have been used in P–E bond forming reactions (E = P, C, Si, B, S), and the metal-mediated reactions often provide facile and safe routes to compounds that are difficult to synthesize by conventional main-group chemistry.²¹ However, Si–H activation by terminal phosphinidenes has not been described.

Results and Discussion

The cationic terminal aminophosphinidene complex $[\text{CpFe}(\text{CO})_2\{\text{PN-}i\text{-Pr}_2\}][\text{AlCl}_4]^-$ (**2**) is readily formed by abstraction of chloride from the chloroaminophosphido complex $[\text{CpFe}(\text{CO})_2\{\text{P}(\text{Cl})\text{N-}i\text{-Pr}_2\}]$ (**1**).¹⁹ Compound **2** reacts at room temperature with primary, secondary, and tertiary silanes, resulting in insertion of the phosphinidene phosphorus into the Si–H bonds and formation of secondary silyl amino phosphine complexes **3–5** (see Scheme 1). In solution, the additions are essentially quantitative. Isolated yields range from 53% to 69%. The reactions of **2** with silanes can be carried out using isolated samples of **2**. Alternately, solutions of **2** can be prepared *in situ* by dissolving **1** and AlCl_3 in dichloromethane. Silanes are then added to the solution to form **3–5**. However, optimal yields and purity are obtained by first dissolving **1** and the silane in CH_2Cl_2 and then adding this solution to solid AlCl_3 . Compound **1** does not react directly with the silane, but reacts with **2** as it is generated *in situ*. All three methods result in the formation of compounds **3–5** as the only significant product.

The resulting compounds have been characterized by ^1H , ^{31}P , and ^{29}Si NMR spectroscopy and infrared spectroscopy. The spectral features of compound **3**, which results from reaction of **2** with PhSiH_3 , will be used to illustrate the general spectral features. The ^1H NMR spectrum of **3** shows a doublet of doublets of doublets at δ 7.82, which corresponds to the P–H. The large $^1J_{\text{PH}}$ coupling of 386.6 Hz indicates a direct P–H bond. Small couplings of 4.4 and 4.1 Hz are observed to two diastereotopic silicon-bound hydrogen atoms. The two Si–H resonances appear at δ 5.02 and 4.87 and are coupled to each other (5.9 Hz), to phosphorus (20.5 and 31.1 Hz, respectively), and to the P–H (4.4 and 4.1 Hz). The ^1H NMR shows additional peaks for the phenyl group, the cyclopentadienyl ligand, and the isopropyl groups

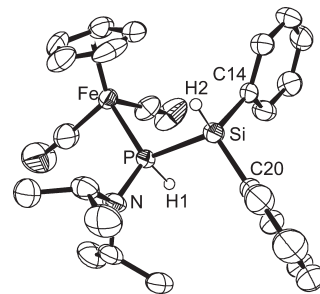


Figure 1. ORTEP diagram showing the crystal structure of $[\text{CpFe}(\text{CO})_2\{\text{P}(\text{H})(\text{SiHPh}_2)(\text{N-}i\text{-Pr}_2)\}][\text{AlCl}_4]^-$ (**4**). Thermal ellipsoids are shown at the 50% level. Hydrogen atoms, except those on P and Si, and the AlCl_4^- counterion have been omitted. Selected distances (Å) and angles (deg): Fe–P = 2.2522(6), Si–P = 2.2927(6), P–N = 1.669(2), N–P–Fe = 121.48(8), N–P–Si = 109.03(8), Fe–P–Si = 113.14(3), C20–Si–C14 = 113.2(1), C20–Si–P = 109.77(8), C14–Si–P = 107.99(7).

on the amine substituent. The ^{31}P NMR of **3** shows a singlet at δ 13.0, while the ^{29}Si spectrum shows a doublet at δ 34.1, with an Si–P coupling of 38 Hz. Silicon satellite peaks are also apparent in the ^{31}P spectrum, and their coupling constant matches the ^{31}P coupling constant observed in the ^{29}Si spectrum. The Si–P, P–H, and H–H couplings clearly establish the formation of the new Si–P bond.

The infrared spectrum of **3** shows carbonyl stretching frequencies of 2064 and 2021 cm^{-1} and a band at 2146 cm^{-1} that is attributed to the Si–H stretch. The observed carbonyl stretching frequencies are comparable to those of known analogous $\text{CpFe}(\text{CO})_2(\text{PR}_3)^+$ complexes.²² For comparison, the carbonyl stretching frequencies of the phosphinidene complex **2** are 2074 and 2036 cm^{-1} . The shift to lower frequency upon silane addition suggests that the silyl phosphine ligand in **3** is a stronger donor and weaker acceptor than the phosphinidene ligand in **2**.

The compound $[\text{CpFe}(\text{CO})_2\{\text{P}(\text{H})(\text{SiHPh}_2)(\text{N-}i\text{-Pr}_2)\}][\text{AlCl}_4]^-$ (**4**) has been structurally characterized. An ORTEP diagram of the X-ray crystal structure is shown in Figure 1. The cation consists of a $\text{CpFe}(\text{CO})_2$ fragment coordinated by an amino-silyl secondary phosphine. The P–Si bond length of 2.2927(6) Å is typical for P–Si single bonds,²³ and the substituents on the tetrahedral P and Si centers are staggered, with the two H substituents in *anti* positions (H–P–Si–H dihedral angle = 178°). The P–N bond length of 1.669(2) Å is consistent with a nitrogen–phosphorus single bond.²⁴ This distance is significantly longer than the typical P–N distance in analogous amino-phosphinidene complexes (1.629–1.634 Å).¹⁶ The lengthening of the P–N bond upon reaction with the silane results from the loss of the N-to-P π -donation that stabilizes the phosphinidene (see below). Similar lengthening of the P–N bond has been observed upon reaction of related amino-phosphinidene complexes with phosphines^{7,17} and alkynes.⁹

(22) Davison, A.; Green, M. L. H.; Wilkinson, G. *J. Chem. Soc.* **1961**, 3172. Kückmann, T. I.; Dornhaus, F.; Bolte, M.; Lerner, H.-W.; Holthausen, M. C.; Wagner, M. *Eur. J. Inorg. Chem.* **2007**, 2007, 1989. McNamara, W. F.; Reisacher, H. U.; Duesler, E. N.; Paine, R. T. *Organometallics* **2002**, 7, 1313.

(23) Chen, T.; Jackson, J.; Jasper, S. A.; Duesler, E. N.; Nöth, H.; Paine, R. T. *J. Organomet. Chem.* **1999**, 582, 25. Plass, W.; Schwarz, W. Z. *Anorg. Allg. Chem.* **1996**, 622, 1786. McCampbell, T. A.; Kinkel, B. A.; Miller, S. M.; Helm, M. L. *J. Chem. Cryst.* **2006**, 36, 271.

(24) Orpen, A. G.; Brammer, L.; Allen, F. H.; Kennard, O.; Watson, D. G.; Taylor, R. *J. Chem. Soc., Dalton Trans.* **1989**, S1.

(21) Waterman, R. *Dalton Trans.* **2009**, 18.

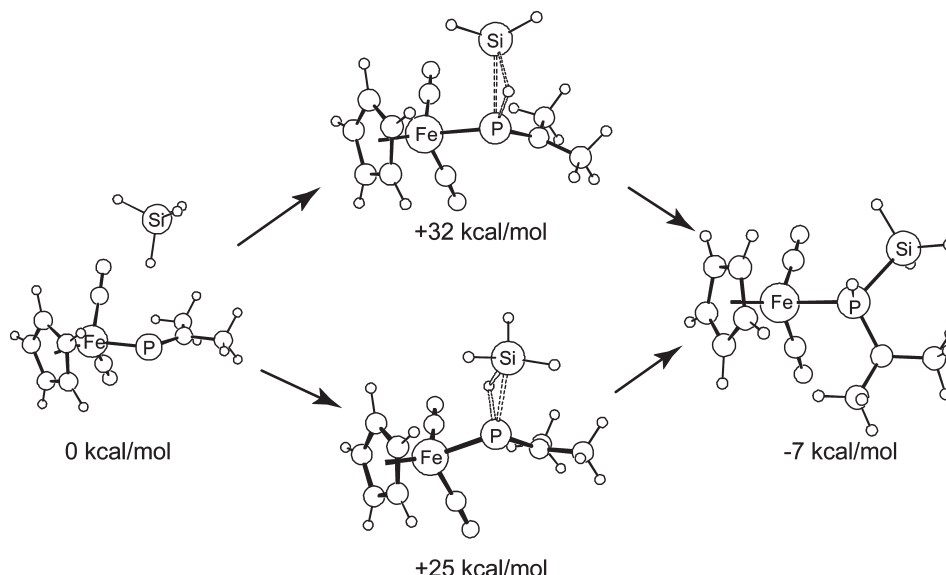


Figure 2. Calculated geometries for the addition of SiH_4 to $[\text{CpFe}(\text{CO})_2(\text{PNMe}_2)]^+$. Selected distances (\AA) and angles (deg) in transition state 1 (+25 kcal/mol): Si–P = 2.62, Si–H = 1.85, P–H = 1.50. P–Si–H = 33.9, Si–P–H = 43.7, P–H–Si = 102.4. Selected distances (\AA) and angles (deg) in transition state 2 (+32 kcal/mol): Si–P = 2.47, Si–H = 1.75, P–H = 1.59. P–Si–H = 40.0, Si–P–H = 45.0, P–H–Si = 95.0.

The Si–H activation reaction has been examined computationally using SiH_4 addition to $[\text{CpFe}(\text{CO})_2\{\text{PN}(\text{CH}_3)_2\}]$ as a model system and Gaussian 03²⁵ with density functional theory B3LYP²⁶ and orbital basis sets LANL2DZ for the Fe atom and 6-31G(d) for other atoms.²⁵ The addition of SiH_4 to $[\text{CpFe}(\text{CO})_2\{\text{PN}(\text{CH}_3)_2\}]$ was found to be concerted, occurring via a triangular transition state. No intermediates were identified. Calculated reactant, transition state, and product geometries are shown in Figure 2. The overall reaction is exergonic by 7 kcal/mol. Two possible pathways and transition states were identified, with activation barriers of 25 and 32 kcal/mol. The transition states differ in the orientation of the silane relative to the phosphinidene (Figure 3). Mulliken partial charges for the key atoms in reactants, transition state, and product are shown in Table 1, and selected distances are given in Table 2.

The bonding in the electrophilic phosphinidene is viewed as being analogous to the bonding in a Fischer carbene. The phosphinidene ligand can be considered to be formally derived from free singlet phosphinidene, which donates one lone pair to the cationic iron center. This leaves on phosphorus a second lone pair and an empty p_z orbital perpendicular to the

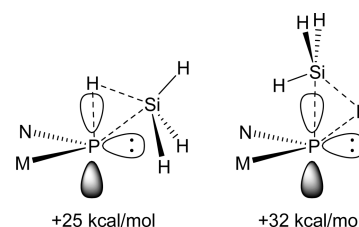


Figure 3. Schematic representation of silane orientation in two calculated transition states.

Table 1. Calculated Mulliken Partial Charges for Key Atoms in Si–H Activation Reaction

	reactant	transition state ^a	product
Fe	−0.708	−0.639	−0.679
P	0.585	0.438	0.482
H	−0.118	−0.071	0.02
Si	0.265	0.381	0.337
N	−0.417	−0.473	−0.498

^a Transition state values are those of the lower energy transition state.

Table 2. Selected Distances (\AA) in Optimized Reactant, Transition State, and Product

	reactant	transition state ^a	product
Fe–P	2.193	2.352	2.293
P–N	1.650	1.679	1.706
Si–H	1.497	1.485	
P–H		1.591	1.429
Si–P		2.469	2.297

^a Transition state values are those of the lower energy transition state.

plane formed by Fe, P, and N. The empty p_z orbital is stabilized by π -donation from the N lone pair and π -back-donation from an appropriate filled metal d orbital.²⁷ Thus, in the starting phosphinidene complex, the positive charge is

(25) Frisch, M. J.; Trucks, G. W.; Schlegel, H. B.; Scuseria, G. E.; Robb, M. A.; Cheeseman, J. R.; Montgomery, J. A., Jr.; Vreven, K. N. K.; J. C. Burant, J. M. M.; Iyengar, S. S.; Tomasi, J.; V. B.; Mennucci, B.; Cossi, M.; Scalmani, G.; Rega, N.; Petersson, G. A.; Nakatsuji, H.; Hada, M.; Ehara, M.; Toyota, K.; Fukuda, R.; Hasegawa, J.; Ishida, M.; Nakajima, T.; Honda, Y.; Kitao, O.; Nakai, H.; Klene, M.; Li, X.; Knox, J. E.; Hratchian, H. P.; Cross, J. B.; Bakken, V.; Adamo, C.; Jaramillo, J.; Gomperts, R.; Stratmann, R. E.; Yazyev, O.; Austin, A. J.; Cammi, R.; Pomelli, C.; Ochterski, J. W.; Ayala, P. Y.; Morokuma, K.; Voth, G. A.; Salvador, P.; Dannenberg, J. J.; Zakrzewski, V. G.; Dapprich, S.; Daniels, A. D.; Strain, M. C.; Farkas, O.; Malick, D. K.; Rabuck, A. D.; Raghavachari, K.; Foresman, J. B.; Ortiz, J. V.; Cui, Q.; Baboul, A. G.; Clifford, S.; Cioslowski, J.; Stefanov, B. B.; Liu, G.; Liashenko, A.; Piskorz, P.; Komaromi, I.; Martin, R. L.; Fox, D. J.; Keith, T.; Al-Laham, M. A.; Peng, C. Y.; Nanayakkara, A.; Challacombe, M.; Gill, P. M. W.; Johnson, B.; Chen, W.; Wong, M. W.; Gonzalez, C.; Pople, J. A. *Gaussian 03, Revision C.02*; Gaussian, Inc.: Wallingford, CT, 2004.

(26) Becke, A. D. *J. Chem. Phys.* **1993**, *98*, 5648. Lee, C.; Yang, W.; Parr, R. G. *Phys. Rev. B* **1988**, *37*, 785.

(27) Grigoleit, S.; Alijah, A.; Rozhenko, A. B.; Streubel, R.; Schoeller, W. W. *J. Organomet. Chem.* **2002**, *643–644*, 223. Ehlers, A. W.; Baerends, E. J.; Lammertsma, K. *J. Am. Chem. Soc.* **2002**, *124*, 2831.

primarily localized on the P as a result of the P→Fe donor interaction, with some positive charge delocalized onto N as a result of N-to-P π -donation and some back onto the metal through π -back-donation.²⁸ Nucleophilic attack is expected to occur at the empty phosphorus p_z orbital, and in the calculated transition states, the silane nucleophile approaches the phosphinidene from this direction (Figure 2). Of the two calculated transition states, the lower energy state is the one in which the Si is oriented toward the phosphorus lone pair and the H is oriented toward the p_z orbital (Figure 3). The preferred orientation thus aligns the partially positive silicon atom with the phosphorus lone pair, and the partially negative hydrogen atom with the empty p_z orbital.

In the transition state, approach of the silane nucleophile decreases the charge at P, as the empty p_z orbital overlaps with the incoming filled Si–H bonding orbital. The charge on N also decreases because N-to-P π -donation to the phosphorus p_z orbital is displaced by the incoming nucleophile. Upon formation of the final product, the charge at phosphorus again increases as the electropositive SiH₃ fragment is added to P. However, the charge at N does not increase from transition state to product because the positive charge at P can no longer be delocalized onto N, as there is no longer an empty p_z orbital on P capable of accepting π -donation from N. For the same reasons, the calculated P–N distance (Table 2) increases from the reactant phosphinidene (1.650 Å) to the transition state (1.679 Å) to the product (1.706 Å) as the N-to-P π -donor interaction is displaced by the incoming nucleophile. This increase correlates well with the P–N bond distance increase observed experimentally upon Si–H addition to the phosphinidene (see above). Calculated Fe–P distances also increase from reactant to product as π -back-donation from iron to the phosphorus p_z orbital is eliminated.

A comparison of the iron partial charges suggests that the silyl phosphine in the product is a weaker donor/stronger acceptor than the phosphinidene in the starting material. However, this is not corroborated by IR spectroscopy, where the formation of the silyl phosphine results in a shift of the carbonyl stretching bands to lower frequency (**2**: 2074, 2036 cm^{-1} , **4**: 2064, 2021 cm^{-1}). The experimental infrared data support our bonding model because the loss of Fe-to-P back-donation upon reaction of the phosphinidene with silane will lead to an increase in Fe to carbonyl back-donation and a corresponding decrease in carbonyl stretching frequency.

For comparison, insertion of the phosphinidene into the C–H bond of methane and the H–H bond of dihydrogen was also studied. Like the Si–H insertion, both of these reactions are concerted and exergonic, with ΔG values of –7 and –11 kcal/mol, respectively. However, the activation barriers of 52 and 40 kcal/mol are significantly higher than that of the Si–H insertion, suggesting that modification of the phosphinidene complex to increase electrophilicity will be necessary to achieve C–H or H–H activation.

Bond activation by electrophilic phosphinidene complexes is well established. Transient phosphinidenes have been shown to react with X–H bonds and have been trapped by water, alcohols, and amines. These reactions likely occur via initial coordination of the N or O lone pair to P, followed by

(28) An alternative, equivalent description of the phosphinidene complex is a metallaphosphenium ion, with the positive charge localized on P and a nondative bond between P and Fe.

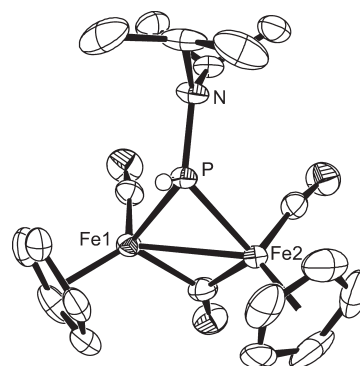
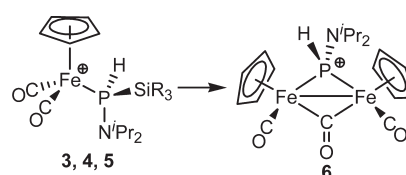


Figure 4. ORTEP diagram showing the crystal structure of [$\{\text{CpFe}(\text{CO})_2(\mu\text{-CO})\{\mu\text{-P}(\text{H})\text{N-}i\text{-Pr}_2\}\}[\text{AlCl}_4]$] (**6**). Thermal ellipsoids are shown at the 50% level. Hydrogen atoms, except the one on P, and the AlCl_4^- counterion have been omitted. Selected distances (Å) and angles (deg): Fe(1)–P = 2.1751(8), Fe(2)–P = 2.1897(8), P–N = 1.651(2), N–P–Fe(1) = 127.9(1), N–P–Fe(2) = 127.7(1), Fe(1)–P–Fe(2) = 73.37(2).

Scheme 2



proton transfer, although the mechanism has not been studied in detail.⁶ A similar mechanism has been described for C–Br activation by phosphinidenes, where the initial step is coordination of a Br lone pair to P, followed by bond insertion.¹² Silanes, however, lack lone pairs so the initial Lewis acid/base coordination is not possible and the addition to the phosphinidene is concerted.

Attempts to explore the reaction chemistry of the silyl phosphine complexes were generally unsuccessful, as the silyl phosphine complexes are extremely sensitive to P–Si bond cleavage. Most reactions attempted led to loss of the silyl group and formation of the bridging phosphido complex [$\{\text{CpFe}(\text{CO})_2(\mu\text{-CO})\{\mu\text{-P}(\text{H})\text{N-}i\text{-Pr}_2\}\}[\text{AlCl}_4]$] (**6**) (Scheme 2). Compound **6** was also observed during attempts to crystallize the silyl phosphine complexes, presumably as a result of reactions with trace water. It is structurally analogous to several known di-iron bridging phosphido complexes.^{29,30} Di-iron and iron-group VI heterobimetallic complexes containing bridging $i\text{-Pr}_2\text{NPH}$ phosphido groups have also been described.³¹

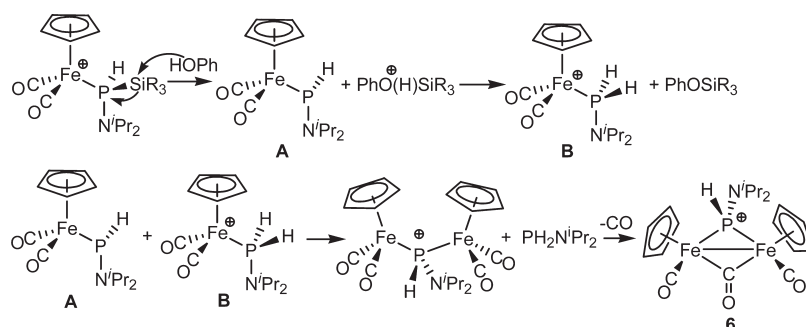
Compound **6** can be formed rationally and in good yield by reaction of any of the silyl phosphine complexes with phenol, allowing us to propose a mechanism for the decomposition

(29) Decken, A.; Bottomley, F.; Wilkins, B. E.; Gill, E. D. *Organometallics* **2004**, *23*, 3683. Lorenz, I.-P.; Pohl, W.; Nöth, H.; Schmidt, M. *J. Organomet. Chem.* **1994**, *475*, 211. Pfeiffer, M.; Stey, T.; Jehle, H.; Klupfel, B.; Malisch, W.; Stalke, D.; Chandrasekhar, V. *Chem. Commun.* **2001**, 337. Decken, A.; Neil, M. A.; Dyker, C. A.; Bottomley, F. *Can. J. Chem.* **2002**, *80*, 55. Fenske, D.; Schottmüller, H. *Z. Anorg. Allg. Chem.* **1998**, *624*, 443. Sugiura, J.; Kakizawa, T.; Hashimoto, H.; Tobita, H.; Ogino, H. *Organometallics* **2005**, *24*, 1099.

(30) Lorenz, I.-P.; Maier, M.; Polborn, K. *Eur. J. Inorg. Chem.* **2002**, *2002*, 327.

(31) Li, Y. W.; Newton, M. G.; King, R. B. *Inorg. Chem.* **2002**, *32*, 5720. Kumar, V.; Lee, D. W.; Newton, M. G.; King, R. B. *J. Organomet. Chem.* **1996**, *512*, 1. King, R. B.; Fu, W. K.; Holt, E. M. *Inorg. Chem.* **2002**, *25*, 2394. King, R. B.; Fu, W. K.; Holt, E. M. *Inorg. Chem.* **2002**, *24*, 3094.

Scheme 3



of the silyl phosphines as shown in Scheme 3. Initial nucleophilic attack by phenol at Si breaks the P–Si bond. The leaving group is a neutral iron phosphido complex **A**, which is then protonated to form the primary aminophosphine complex **B**. In the reaction of **5** ($\text{SiR}_3 = \text{SiEt}_3$) with phenol, the side product PhOSiEt_3 was identified by GC-MS ($m/z = 208$) and was the only significant volatile component of the reaction mixture. Support for the intermediacy of **B** comes from its observation as a fragment in electrospray mass spectra of all of the silyl phosphine complexes, where it likely forms through reaction of the silyl phosphine with adventitious water. Attempts to observe or isolate **B** in solution were not successful. Direct experimental evidence for the final dimerization step of the mechanism could not be found, as the proposed side product, $\text{PH}_2\text{N-}i\text{-Pr}_2$, was not observed in solution. This compound has been synthesized but is known to be unstable and likely decomposes under our reaction conditions.³² However, support for this step of the mechanism comes from related work, where hydrolysis of P–Si bonds in silyl phosphine complexes has been used to form bridging phosphido complexes.³⁰

In summary, we have shown that terminal electrophilic phosphinidene complexes activate Si–H bonds, resulting in insertion of phosphorus in the Si–H bond and leading to secondary silyl phosphines. The addition occurs via a concerted mechanism and results in the formation of a new P–Si bond, as well as a P–H bond, which may serve as a site for further functionalization. This reaction represents a facile new method of P–Si bond formation.

Experimental Section

General Comments. All procedures were carried out under a nitrogen atmosphere using standard Schlenk techniques or in an inert atmosphere glovebox. THF was distilled from Na/benzophenone. Dichloromethane and hexane were purified using solvent purification columns containing alumina (dichloromethane) or alumina and copper catalyst (hexane). Deuterated chloroform was distilled from P_2O_5 . The NMR spectra were recorded in CDCl_3 or CD_2Cl_2 using a Varian Mercury 300 at 300.179 MHz (^1H), 121.515 MHz ($^{31}\text{P}\{^1\text{H}\}$), or 59.637 MHz ($^{29}\text{Si}\{^1\text{H}\}$). Infrared spectra were recorded in CH_2Cl_2 solution. Compounds **3**, **4**, and **5** are extremely water sensitive, and crystalline samples rapidly revert to oils upon supernatant removal. As a result, satisfactory elemental analysis could not be obtained for these compounds. However, their formulations and purity are well supported by mass spectrometry and spectroscopy. Mass spectra of metal complexes were carried out using a Finnigan-Matt TSQ-700 mass spectrometer equipped with electrospray ionization and a Harvard syringe pump.

GC-MS experiments were carried out using a Finnigan-Matt INCOS 50 connected to an HP-5890A gas chromatograph equipped with a J&W DB-5MS column. The MS was operated in positive ion mode with electron impact ionization.

a. Synthesis of $[\text{CpFe}(\text{CO})_2\{\text{P}(\text{Cl})\text{N-}i\text{-Pr}_2\}]$ (1**).** This compound was synthesized using a modification of the published procedure.¹⁹ Excess sodium/potassium alloy ($\text{NaK}_{2.8}$, 2.0 mL, 1.14 g, 24 mmol K) was added to a vigorously stirred solution of $[\text{CpFe}(\text{CO})_2]_2$ (1.0 g, 2.8 mmol) in THF (75 mL). The mixture was stirred for 3 h and then filtered via inverse filtration. The filtrate was added in small portions via canula to a solution of $\text{Cl}_2\text{PN-}i\text{-Pr}_2$ (1.06 mL, 1.44 g, 7.2 mmol) in THF (75 mL) at -78°C . After the addition was complete, the solution was warmed to room temperature and stirred for 30 min. The solvent was removed *in vacuo*, and the residue was extracted into pentane (5×10 mL). The pentane extracts were filtered and cooled to -25°C for 24 h, resulting in the formation of red-orange crystals. The supernatant was decanted and the solid was dried *in vacuo*. Yield: 0.90 g, 46%.

b. Synthesis of $[\text{CpFe}(\text{CO})_2\{\text{PN-}i\text{-Pr}_2\}][\text{AlCl}_4]$ (2**).** This compound was synthesized using a modification of the published procedure.¹⁹ In a typical experiment, a solution of **2** was prepared by dissolving $[\text{CpFe}(\text{CO})_2\{\text{P}(\text{Cl})\text{N-}i\text{-Pr}_2\}]$ (**1**) (30 mg, 0.087 mmol) and AlCl_3 (17 mg, 0.13 mmol) in CH_2Cl_2 (0.5 mL) and then reacted *in situ*. Conversion of **1** to **2** is essentially quantitative by NMR spectroscopy. Compound **2** is not routinely isolated because it is extremely air and water sensitive, and isolated yields are poor.

c. Synthesis of $[\text{CpFe}(\text{CO})_2\{\text{P}(\text{H})(\text{SiH}_2\text{Ph})(\text{N-}i\text{-Pr}_2)\}][\text{AlCl}_4]$ (3**).** The compound $[\text{CpFe}(\text{CO})_2\{\text{P}(\text{Cl})\text{N-}i\text{-Pr}_2\}]$ (50 mg, 0.146 mmol) was dissolved in CH_2Cl_2 (2 mL), and H_3SiPh (36.0 μL , 0.292 mmol) was then added. The resulting solution was added to AlCl_3 (29.2 mg, 0.219 mmol) and stirred for 30 min. Pentane (5 mL) was added slowly with mixing, and the resulting cloudy solution was cooled at -30°C for 3 days, resulting in the formation of a red oil and yellow-orange crystals. The supernatant was decanted, and the oil was triterated with pentane (3×1 mL), resulting in the formation of a semicrystalline oily solid, which was dried under vacuum. Yield: 45 mg, 53%. IR (CH_2Cl_2 solution, cm^{-1}): $\nu_{\text{Si-H}} = 2146$; $\nu_{\text{CO}} = 2064, 2021$. ^1H NMR: δ 7.82 (ddd, 1H, PH, $^1J(\text{HP}) = 386.6$ Hz, $^3J(\text{HH}) = 4.1, 4.4$ Hz), 7.8–7.4 (m, Ph), 5.17 (s, 5H, C_5H_5), 5.02 (ddd, 1H, SiH, $^2J(\text{HP}) = 20.5$ Hz, $^2J(\text{HH}) = 5.9$ Hz, $^3J(\text{HH}) = 4.1$ Hz), 4.87 (ddd, 1H, SiH, $^2J(\text{HP}) = 31.1$ Hz, $^2J(\text{HH}) = 5.9$ Hz, $^3J(\text{HH}) = 4.4$ Hz), 3.28 (sept, 1H, $\text{CH}(\text{CH}_3)_2$, $^3J(\text{HH}) = 6.6$ Hz), 3.24 (sept, 1H, $\text{CH}(\text{CH}_3)_2$, $^3J(\text{HH}) = 6.3$ Hz), 1.19 (doublet, 6H, $\text{CH}(\text{CH}_3)_2$, $^3J(\text{HH}) = 6.3$ Hz), 1.09 (doublet, 6H, $\text{CH}(\text{CH}_3)_2$, $^3J(\text{HH}) = 6.6$ Hz). ^{31}P NMR: δ 13.0 (s w satellites, $^1J_{\text{SiP}} = 38$ Hz). ^{29}Si NMR: 34.1 (d, $^1J_{\text{SiP}} = 38$ Hz). MS (electrospray, CH_2Cl_2 solution): $m/z = 416$ (M^+), 308 ($\text{M} - \text{SiH}_3\text{Ph}^+$). Note: although compounds **3–5** are routinely synthesized by generating the phosphinidene complex **2** in the presence of the silane, they can also be formed by first synthesizing and isolating **2** and then reacting it with silane. The procedure described above gives better yields and purity.

d. Synthesis of [CpFe(CO)₂{P(H)(SiHPh₂)N-*i*-Pr₂}] [AlCl₄] (**4**). The compound [CpFe(CO)₂(P(Cl)N-*i*-Pr₂)] (50 mg, 0.146 mmol) was dissolved in CH₂Cl₂ (0.5 mL), and H₂SiPh₂ (54.2 μL, 0.292 mmol) was then added. The resulting solution was added to AlCl₃ (29.2 mg, 0.219 mmol) and stirred for 30 min. Pentane (5 mL) was added slowly with mixing, and the resulting cloudy solution was cooled at -30 °C for 4 days, resulting in the formation of a dark orange oil. The supernatant was decanted, and the oil was triterated with pentane (3 × 1 mL), resulting in the formation of a semicrystalline oily solid, which was dried under vacuum. Yield: 66 mg, 68%. IR (CH₂Cl₂ solution, cm⁻¹): ν_{PH} = 2251, ν_{SiH} = 2146, ν_{CO} = 2064, 2021. ¹H NMR: δ 7.62 (dd, 1H, ¹J(HP) = 350 Hz, ³J(HH) = 6 Hz, PH), 7.3–7.9 (m, Ph), 5.53 (dd, 1H, ²J(PH) = 28 Hz, ³J(HH) = 6 Hz, SiH), 3.2 (d sept, 2H, ³J(HH) = 7 Hz, ³J(HP) = 16 Hz, CH(CH₃)₂), 1.19 (d, ³J(HH) = 7 Hz, CH₃), 0.91 (d, ³J(HH) = 7 Hz, CH₃). ³¹P{¹H} NMR: δ 15.9 (s w satellites, ¹J(SiP) = 36 Hz). ²⁹Si{¹H} NMR: δ -9.8 (d, ¹J(SiP) = 36 Hz). MS (electrospray, CH₂Cl₂ solution): *m/z* = 492 (M⁺), 310 (M - SiPh₂)⁺, 308 ([M - H₂SiPh₂]⁺).

e. Synthesis of [CpFe(CO)₂{P(H)(SiEt₃)N-*i*-Pr₂}] (**5**). The compound [CpFe(CO)₂(P(Cl)N-*i*-Pr₂)] (50 mg, 0.146 mmol) was dissolved in CH₂Cl₂ (0.5 mL), and HSiEt₃ (46.6 μL, 0.292 mmol) was then added. The resulting solution was added to AlCl₃ (23.4 mg, 0.175 mmol) and mixed well. Pentane (5 mL) was added slowly, and the resulting solution was kept at -30 °C for 4 days, resulting in the formation of an orange precipitate. The supernatant was decanted, and the solid was washed with pentane and then dried under vacuum. Yield: 60 mg, 69%. IR (CH₂Cl₂ solution, cm⁻¹): ν_{PH} = 2223, ν_{CO} = 2062, 2019. ¹H NMR: δ 7.26 (d, 1H, PH, ¹J(HP) = 340 Hz), 5.35 (s, 5H, C₅H₅), 3.21 (d sept, 2H, CH(CH₃)₂, ³J(HH) = 6.6 Hz, ³J(HP) = 15 Hz), 1.22 (d, 6H, CH(CH₃)₂, ³J(HH) = 6.6 Hz), 1.21 (d, 6H, CH(CH₃)₂, ³J(HH) = 6.6 Hz), 1.16 (t, 9H, SiCH₂CH₃, ³J(HH) = 7.5 Hz), 0.58 (q, 6H, SiCH₂, ³J(HH) = 7.5). ³¹P{¹H} NMR: δ 9.9 (s w satellites, ¹J(SiP) = 20 Hz). ²⁹Si{¹H} NMR: δ 24.1 (d, ¹J(SiP) = 20 Hz). MS (electrospray, CH₂Cl₂ solution): *m/z* = 424 (M⁺), 310 ([M - SiEt₃ + H]⁺).

f. Synthesis of [CpFe(CO)₂{μ-CO}{μ-P(H)N-*i*-Pr₂}] [AlCl₄] (**6**). A solution of [CpFe(CO)₂{P(H)(SiEt₃)(N-*i*-Pr₂)] [AlCl₄] in 2 mL of CH₂Cl₂ was prepared from [CpFe(CO)₂(P(Cl)N-*i*-Pr₂)] (50 mg, 0.146 mmol) as described above. Phenol (8.1 mg, 0.146 mmol) was added, and the resulting solution was stirred for 15 min. The solvent was removed under vacuum, and the residue was extracted into 1 mL of CH₂Cl₂. Pentane (5 mL) was slowly added with stirring, and the resulting slightly cloudy solution was cooled to -30 °C for 15 h, resulting in the formation of a dark red precipitate. The supernatant was decanted, and the precipitate was washed with 3 × 5 mL of pentane, dried under vacuum, and then re-extracted into CH₂Cl₂ (0.3 mL). Pentane (3 mL) was added, and resulting solution was again cooled to -30 °C for 15 h, resulting in the formation of dark red crystals, which were collected and dried under vacuum. Yield: 26 mg, 57%. IR (cast, cm⁻¹): ν_{CO} = 2045, 2037, 2002, 1950, 1823. ¹H NMR: δ 7.15 (dd, 1H, ¹J(HP) = 402 Hz, PH), 5.45 (m, 5H, Cp), 3.7 (bm, 1H, NCH(CH₃)₃), 3.4 (m, 1H, NCH(CH₃)₃), 1.54 (d, 6H, ³J(HH) = 6.3 Hz, CH₃), 1.25 (d, 6H, ³J(HH) = 6.6 Hz, CH₃). ³¹P{¹H} NMR: δ 12.7. MS (electrospray, CH₂Cl₂ solution): *m/z* = 458 (M⁺), 419, 402. **GC-MS.** A solution of [CpFe(CO)₂{P(H)(SiEt₃)N-*i*-Pr₂}] (**5**) (0.058 mmol) in CH₂Cl₂ (2 mL) was prepared as described above. Phenol (5.5 mg, 0.058 mmol) was added, and the resulting solution was stirred for 15 min. A 5 μL aliquot was withdrawn from the solution and injected into the GC-MS. The only significant volatile component observed was PhOSiEt₃ (retention time = 12.5 min, *m/z* = 208 (M⁺), 179 ([M - Et]⁺), 151 ([M - Et - H₂C=CH₂]⁺), 123 ([M - Et - 2 H₂C=CH₂]⁺), 77 (Ph⁺).

g. Computational Chemistry. All calculations were performed using the Gaussian 03 software package, revisions C.02 and E.01.²⁵ The level of approximation was the density-functional theory B3LYP,²⁶ and the orbital basis sets were LANL2DZ for

Table 3. Crystal Data and Structure Refinement for **4** and **6**

	4	6
empirical formula	C ₂₅ H ₃₁ AlCl ₄ -FeNO ₂ PSi	C ₁₉ H ₂₅ AlCl ₄ -Fe ₂ NO ₃ P
fw	661.20	626.85
temperature (K)	173(2)	173(2)
wavelength (Å)	0.71073	0.71073
cryst syst	orthorhombic	monoclinic
space group	<i>Pna</i> 2 ₁	<i>P</i> 2 ₁
unit cell dimens		
<i>a</i> (Å)	24.434(3)	10.321(2)
<i>b</i> (Å)	10.191(1)	12.557(2)
<i>c</i> (Å)	12.795(1)	10.334(2)
β (deg)		98.259(2)
volume (Å ³)	3186.0(6)	1325.5(4)
<i>Z</i>	4	2
density (calcd) (Mg/m ³)	1.378	1.571
absorp coeff (mm ⁻¹)	0.947	1.612
<i>F</i> (000)	1360	636
cryst size (mm ³)	0.37 × 0.36 × 0.19	0.53 × 0.26 × 0.26
θ range (deg)	1.67 to 27.48	1.62 to 27.48
index ranges	-31 ≤ <i>h</i> ≤ 31 -13 ≤ <i>k</i> ≤ 13 -16 ≤ <i>l</i> ≤ 16	-13 ≤ <i>h</i> ≤ 13 -16 ≤ <i>k</i> ≤ 16 -13 ≤ <i>l</i> ≤ 13
reflns collected	25 971	11 453
indep reflns	7253 [<i>R</i> (int) = 0.0317]	5979 [<i>R</i> (int) = 0.0160]
completeness to θ = 27.48°	100.0%	99.3%
max. and min transmn data/restraints/params	0.8406 and 0.7208	0.6793 and 0.4821
goodness-of-fit on <i>F</i> ²	7253/1/333	5979/1/287
final <i>R</i> indices [<i>I</i> > 2σ(<i>I</i>)]	1.094	1.067
<i>R</i> 1	0.0330	0.0236
w <i>R</i> 2	0.0722	0.0585
<i>R</i> indices (all data)		
<i>R</i> 1	0.0392	0.0240
w <i>R</i> 2	0.0750	0.0589
absolute struct param	-0.01(1)	
largest diff peak and hole (e Å ³)	0.422 and -0.214	0.485 and -0.374

the Fe atom and 6-31G(d) for all others.²⁵ Transition state structures were located using opt=ts or opt=ts,ef (i.e., no synchronous transit) algorithms. Each optimized transition state structure was subjected to a vibrational frequency analysis, to ensure that the structure was indeed a transition state: there should be 1 imaginary frequency only, and the magnitudes of all frequencies should be greater than the residual noise (the six “zero frequencies” for translations and rotations from normal mode diagonalization). The appropriateness of each located transition state and the single-step nature of the reactions were verified by “plus-and-minus-displacement” minimization runs: the transition state is displaced ~0.05 Å or 5° along the imaginary-frequency normal mode in both directions, and the two displaced structures are optimized toward the nearest minimum-energy structures. Gibbs energies (298.15 K) were computed using the rigid-rotor/harmonic-oscillator assumptions. Partial charges are according to a Mulliken population analysis.

h. X-ray Crystallography. Suitable crystals of compounds **4** and **6** were mounted on glass fibers. Programs for diffractometer operation, data collection, cell indexing, data reduction, and absorption correction were those supplied by Bruker AXS Inc., Madison, WI. Diffraction measurements were made on a PLATFORM diffractometer/SMART 1000 CCD using graphite-monochromated Mo Kα radiation at -100 °C. The unit cell was determined from randomly selected reflections obtained using the SMART CCD automatic search, center, index, and least-squares routines. Integration was carried out using the program SAINT, and an absorption correction was performed using SADABS. Crystal data and collection

parameters are listed in Table 3. Structure solution was carried out using the SHELX97³³ suite of programs and the WinGX graphical interface.³⁴ Initial solutions were obtained by direct methods and refined by successive least-squares cycles. All non-hydrogen atoms were refined anisotropically. During solution of **6**, the PLATON³⁵ routine TWINROT was used to identify a 2-fold twin axis about [1 0 1], which was accounted for with the twin law 0 0 1 0 -1 0 1 0 0. Racemic twinning was also identified, resulting in a total of four twin components.

(33) Sheldrick, G. M. *SHELX97, Programs for Crystal Structure Analysis*, Release 97-2; **1998**.

(34) Farrugia, L. J. *J. Appl. Crystallogr.* **1999**, 32, 837.

(35) Spek, A. L. *J. Appl. Crystallogr.* **2003**, 36, 7.

Acknowledgment. This work was financially supported by NSERC (Discovery Grant to B.T.S.) and the University of Regina. Computations were performed on a supercomputer funded by the CFI (New Opportunities Grant to A.L.L.E.) and Parallel Quantum Solutions, Arkansas (in-kind contribution). We also thank Bob McDonald and Mike Ferguson (University of Alberta) for X-ray data collection, and Ron Treble (University of Regina) for GC-MS analysis.

Supporting Information Available: Tables giving full coordinates, energies, and Mulliken charges for calculated structures, CIF files giving full details of X-ray crystal structures. This material is available free of charge via the Internet at <http://pubs.acs.org>.